

# THE APPARENT SHAPE OF THE “STRÖMGREN SPHERE” AROUND THE HIGHEST REDSHIFT QSOs WITH GUNN-PETERSON TROUGHS

QINGJUAN YU<sup>1</sup>

Department of Astronomy, 601 Campbell Hall, University of California at Berkeley, Berkeley, CA 94720; yqj@astro.berkeley.edu

*Draft version August 19, 2018*

## ABSTRACT

Although the highest redshift QSOs ( $z > 6.1$ ) are embedded in a significantly neutral background universe (mass-averaged neutral hydrogen fraction  $> 1\%$ ) as suggested by the Gunn-Peterson absorption troughs in their spectra, the intergalactic medium in their vicinity is highly ionized. The highly ionized region is generally idealized as spherical and called the Strömgren sphere. In this paper, by combining the expected evolution of the Strömgren sphere with the rule that the speed of light is finite, we illustrate the apparent shape of the ionization fronts around the highest redshift QSOs and its evolution, which depends on the age, luminosity evolution, and environment of the QSO (e.g., the hydrogen reionization history). The apparent shape may systematically deviate from a spherical shape, unless the QSO age is significantly long compared to the hydrogen recombination process within the ionization front and the QSO luminosity evolution is significantly slow. Effects of anisotropy of QSO emission are also discussed. The apparent shape of the “Strömgren sphere” may be directly mapped by transmitted spectra of background sources behind or inside the ionized regions or by surveys of the hyperfine transition (21 cm) line emission of neutral hydrogen.

*Subject headings:* cosmology: theory — early universe — galaxies: high redshift — quasars: general — quasars: absorption lines — relativity

## 1. INTRODUCTION

The existence of the Gunn-Peterson absorption trough in the spectra of the highest redshift QSOs ( $z > 6.1$ ) suggests that hydrogen in the early universe is significantly neutral ( $> 1\%$  in mass average; e.g., Fan et al. 2002; see also Wyithe & Loeb 2004a; Mesinger & Haiman 2004; Yu & Lu 2005). However, hydrogen in the vicinity of the QSOs may be highly ionized by ionizing photons from QSOs (i.e., the proximity effect; e.g., Bajtlik et al. 1988), as indicated in the QSO spectra by the transmission of flux at wavelengths between the Gunn-Peterson trough and the Ly $\alpha$  line center. These highly ionized regions around the QSOs are generally idealized as spherical in the rest frame of the QSO and called Strömgren spheres.<sup>2</sup> The expansion of the Strömgren sphere depends on the QSO luminosity evolution and its environment (e.g., Donahue & Shull 1987; Shapiro & Giroux 1987). Observers on Earth perceive an object (here the highly ionized region) by the light reaching Earth at the same moment. Since the speed of light is finite, the apparent shape of the expanding ionization front around the QSO may not be spherical.

Wyithe & Loeb (2004b) show that the ionization fronts along the line of sight and transverse to it may have different observed sizes (see also discussions on the size along the line of sight in White et al. 2003 and related discussions in Pentericci et al. 2002). In this paper we generalize the time-delay effect to all angles around the highest redshift QSOs and illustrate the expected apparent shape of the surrounding ionization front and its

evolution (for the relativistic time-delay effects in other astrophysical contexts, e.g., see also Couderc 1939; Rees 1966). We show how the shape depends on the QSO luminosity evolution and its environment (such as the neutral hydrogen fraction and clumpiness). Comparison of observations with the model prediction of the apparent shape may provide constraints on QSO properties, the reionization history of the universe, and/or the cosmological parameter  $\Omega_{\Lambda}$  (by the Alcock-Paczynski test; Alcock & Paczyński 1979).

This paper is organized as follows. In § 2, we illustrate the geometry of the time-delay effect on the apparent shape of the ionization front around a QSO. In § 3, we study the evolution of the Strömgren sphere in the QSO rest frame. We combine the evolution and the time-delay effect to illustrate the evolution of the apparent shape of the ionization front in § 4. The effects of anisotropy of QSO emission are discussed in § 5. Possible observational tests of the apparent shape are discussed in § 6. Our conclusions are summarized in § 7.

In reality the boundary of an ionized region may not be exactly round even without considering the relativistic time-delay effect and the QSO anisotropic emission. Since the Strömgren sphere is idealized as spherical by ignoring other possible random fluctuations on the boundary, the apparent shapes shown in this paper are also idealized as smooth and may more appropriately represent the average over the fluctuations.

## 2. GEOMETRY

We use Figure 1 to illustrate the geometry of the apparent shape of the ionization front around a QSO at point  $O$ . For simplicity, we ignore the Hubble expansion within the ionization front, since here the physical size of the ionized region around the highest redshift QSOs is much smaller than the Hubble scale and the

<sup>1</sup> Hubble Fellow

<sup>2</sup> These highly ionized HII regions (or Strömgren spheres) are well defined only for QSOs that have the Gunn-Peterson trough. QSOs with relatively low redshifts do not have an unambiguous Strömgren sphere because their environment has already been highly ionized by stars (e.g., see Adelberger 2004).

characteristic timescale of the QSO luminosity evolution is much smaller than the age of the universe at  $z \sim 6$ . The derivation below is a simple application of the rule that the speed of light is finite. Suppose that the nuclear activity of the QSO is triggered at cosmic time  $t_i$ . The ionizing photons emitted from the QSO will then ionize surrounding neutral hydrogen. For simplicity, we assume that the QSO emission is isotropic here and discuss the anisotropic effect of the emission in § 5. In the rest frame of the QSO, a spherical ionization front will form and expand (see the dotted circles in Fig. 1), separating the inside highly ionized region and the outside neutral or partly neutral region. We denote the physical (proper) radius of the expanding sphere at cosmic time  $t$  ( $\geq t_i$ ) by  $R(t; t_i)$ . The detailed evolution of  $R(t)$  is related to the QSO luminosity evolution and its environment, which will be determined in § 3. The observer on Earth perceives the ionization front by the light reaching Earth at the same moment. If photons emitted from (or passing through) the ionization front, e.g., point  $A$  in Figure 1, reach the distant observer at the same time as photons from the QSO, the photons from  $A$  should be emitted from (or pass through)  $A$  at cosmic time

$$t_A = t(z_Q) + R(t_A) \cos \theta / c, \quad 0 \leq \theta \leq \pi, \quad (1)$$

where  $z_Q$  is the QSO redshift,  $t(z_Q)$  is the cosmic time corresponding to  $z_Q$ ,  $c$  is the speed of light, and  $\theta$  is the angle between  $\overrightarrow{OA}$  and the observer's line of sight  $\overrightarrow{OC}$  (see Fig. 1). For QSO photons to reach the ionization front  $A$  at cosmic time  $t_A$ , they should emit from the QSO  $O$  at an earlier time

$$t_O = t_A - R(t_A)/c. \quad (2)$$

Given any  $t_O$  ( $t_i \leq t_O \leq t_A$ ), the solution of equation (2)  $t_A$  is unique since the expansion speed of  $R(t_A)$  is slower than  $c$ . Thus we may define such a function  $r(\tau; t_i) \equiv R(t_A; t_i)$  by changing the independent variable from  $t_A$  to  $\tau$ , where  $\tau \equiv t_O - t_i$  is the age of the QSO at  $t_O$ . According to the above, the apparent shape of the ionization front ( $r, \theta$ ) should satisfy the following equation:

$$r(\tau)(1 - \cos \theta) = c(\tau_Q - \tau), \quad 0 \leq \theta \leq \pi, \quad (3)$$

where  $\tau_Q \equiv t(z_Q) - t_i$  is the age of the QSO at cosmic time  $t(z_Q)$ . The apparent shape (illustrated by the solid curve in Fig. 1) is rotationally symmetric along the observer's line of sight to the QSO. The shape is generally not a sphere [unless  $r(\tau)$  does not change with  $\tau$ ]. According to equation (3), given  $\tau_Q$  and an increasing function  $r(\tau)$ , the apparent size  $r$  decreases with increasing  $\theta$ . Because of the existence of the term “ $-\tau$ ” in the right-hand side of equation (3), the apparent shape ( $r, \theta$ ) is neither a spheroid (the apparent shape of relativistically expanding spherical shell of radio sources discussed in Rees 1966, 1967) unless  $r(\tau)$  is a linear function of  $\tau$  nor a “light-echo” paraboloid around a nova or supernova (Couderc 1939).

We define the apparent radial expansion speed of the ionization front at a given  $\theta$  by  $v_{\text{app}} \equiv dr'/dt'$ , where  $r' = (1+z)r$  is the comoving distance of  $r$  and  $dt' = (1+z)d\tau_Q$  is the time interval measured by the observer with including the effect of the cosmological time dilation. According to equations (1)–(3), the apparent radial

expansion speed of the ionization front in units of  $c$  at a given  $\theta$  is given by

$$\beta_{\text{app}} \equiv \frac{v_{\text{app}}}{c} = \frac{1}{c} \frac{dr}{d\tau_Q} \bigg|_{\theta} = \frac{dr/d\tau}{c + (dr/d\tau)(1 - \cos \theta)}, \quad (4)$$

$$= \frac{dR/dt_A}{c - (dR/dt_A) \cos \theta}. \quad (5)$$

Note that the physical expansion speed of the ionization front in the QSO rest frame is

$$dR/dt_A = (dr/d\tau)/(1 + c^{-1}dr/d\tau) < c, \quad (6)$$

which is consistent with special relativity that real information does not travel faster than the speed of light. If  $dR/dt_A$  is highly relativistic, the apparent expansion is superluminal at sufficiently small  $\theta$ , i.e.,  $\beta_{\text{app}} > 1$ , and  $\beta_{\text{app}}$  is close to  $1/2$  when  $\theta \rightarrow \pi$ . We can also define the apparent transverse expansion speed in units of  $c$  through  $\beta_{\text{app}, \perp} \equiv \beta_{\text{app}} \sin \theta$ , which gives the conventionally transverse superluminal phenomenon at sufficiently small  $\theta$  if  $dR/dt_A \rightarrow c$ . According to equation (5), the lower limit on the QSO lifetime can be constrained simply by the apparent sizes of the ionization front, e.g.,  $\tau_Q > 2r(\theta = \pi)/c$  or  $\tau_Q > r(\theta = \pi/2)/c$ .

### 3. THE EVOLUTION OF $r(\tau)$

We denote the mean neutral hydrogen fraction in the region surrounding the QSO prior to the triggering of its nuclear activity by  $x_{\text{HI}} \equiv \langle n_{\text{HI}} \rangle / \langle n_{\text{H}} \rangle$  ( $\sim$  several percent to 10–20% in Yu & Lu 2005; and the rest of the hydrogen has been ionized by stars or collisionally ionized in large halos; also cf., Mesinger & Haiman 2004 or for a higher fraction Wyithe & Loeb 2004a), where  $\langle n_{\text{HI}} \rangle$  is the average proper number density of neutral hydrogen and  $\langle n_{\text{H}} \rangle$  is the density of total hydrogen. After the nuclear activity is triggered, the expansion of the ionization front (or the Strömgren sphere) in the rest frame of the QSO as a function of  $\tau$  (not as a function of  $t_A$  here) may be described by the following equation (e.g., Donahue & Shull 1987; Shapiro & Giroux 1987; Cen & Haiman 2000; Madau & Rees 2000; Yu & Lu 2005):

$$\frac{4\pi}{3} \frac{d(x_{\text{HI}} \langle n_{\text{H}} \rangle r^3)}{d\tau} = \dot{N}_{\text{phs}}(\tau) - \frac{4\pi}{3} \alpha_{\text{B}} C \langle n_{\text{H}} \rangle^2 r^3, \quad (7)$$

where  $\dot{N}_{\text{phs}}(\tau)$  is the ionizing photon emission rate of the QSO at its age  $\tau$ ,  $\alpha_{\text{B}} (= 2.6 \times 10^{-13} \text{ cm}^3 \text{ s}^{-1}$  at  $T = 10^4 \text{ K}$ ) is the hydrogen recombination coefficient to excited levels of hydrogen,  $C \equiv \langle n_{\text{HI}}^2 \rangle / \langle n_{\text{H}} \rangle^2$  is the clumping factor describing the effective clumpiness of hydrogen ionized by QSO photons, and “ $\langle \cdot \cdot \cdot \rangle$ ” represents the space average over the sphere with radius  $r$ . Note that here  $C$  is a little different from the conventional definition of  $\langle n_{\text{HI}}^2 \rangle / \langle n_{\text{H}} \rangle^2$ . The second term on the right-hand side of equation (7) accounts for the recombination of ionized hydrogen within the Strömgren sphere. In equation (7) we set the parameters ( $x_{\text{HI}}, \langle n_{\text{H}} \rangle, C$ ) to be the values at cosmic time  $t = t_i + \tau$ , and their changes during the time interval  $r/c$  of the QSO photon propagation in the Strömgren sphere have been assumed to be negligible. For simplicity, we also neglect their dependence on  $r$  and set them to be constants in the calculations below. Thus, the solution of equation (7) is given by

$$r(\tau) = \left[ \frac{3}{4\pi \langle n_{\text{H}} \rangle x_{\text{HI}}} \int_0^{\tau} \dot{N}_{\text{phs}}(\tau') \exp\left(\frac{\tau' - \tau}{\tau_{\text{rec}}}\right) d\tau' \right]^{1/3} \quad (8)$$

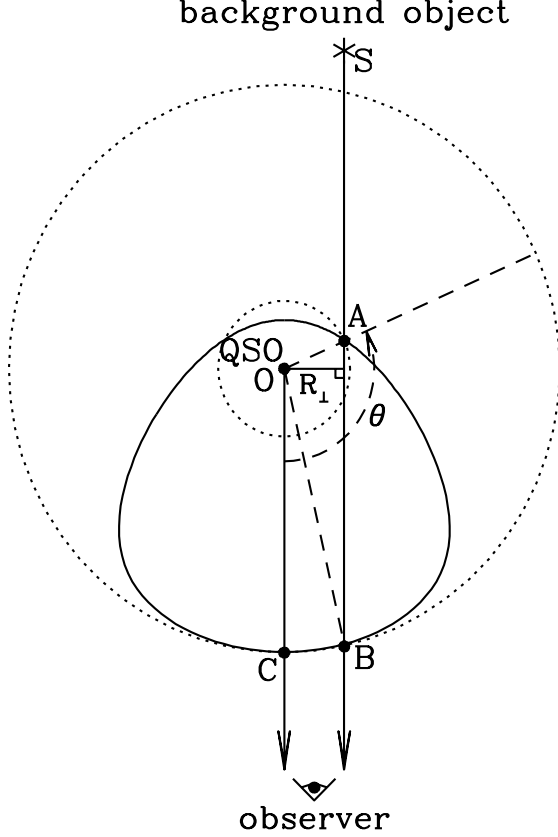


FIG. 1.— Schematic diagram for the apparent shape of the ionization front around a QSO (with the Gunn-Peterson trough in the spectrum). The QSO is at point  $O$  and the distant observer on Earth is located in the direction of  $OC$ . The QSO emission is assumed to be isotropic. The dotted circles represent the ionization fronts at a given cosmic time ( $t_A$  and  $t_B$  for inside and outside circles, respectively) in the rest frame of the QSO. Hydrogen inside the circle (or the Strömgren sphere) is highly ionized by QSO photons. The solid curve is the apparent ionization front, which follows equation (3). Photons emitted from (or passing through) the apparent ionization front (e.g., from point  $A$  at  $t_A$  and  $B$  at  $t_B$  shown in this figure) reach the observer at the same time. The apparent shape of the ionization front is rotationally symmetric along  $OC$  and is generally not a sphere/spheroid/paraboloid. The apparent shape could be mapped by observational spectra of background objects (e.g.,  $S$  in the figure) or the tomograph of H I 21 cm line emission.

where the recombination timescale

$$\tau_{\text{rec}} \equiv x_{\text{HI}}(C\langle n_{\text{H}} \rangle \alpha_{\text{B}})^{-1} \simeq 4 \times 10^6 \text{ yr} \left( \frac{x_{\text{HI}}}{0.1} \right) \left( \frac{30}{C} \right) \left( \frac{7.4}{1+z} \right)^3 \quad (9)$$

characterizes the role of the recombination term in equation (7).

The physical expansion of the ionization front in the rest frame of the QSO  $dR/dt_A$  was discussed in White et al. (2003) by accounting for finite light travel time and ignoring the recombination terms, and was generalized in equation (1) of Wyithe & Loeb (2004a). Here applying equation (7) into equation (6), we obtain the physical expansion of the ionization front as follows:

$$\frac{dR}{dt_A} = c \frac{\dot{N}_{\text{phs}} - \frac{4\pi}{3} \alpha_{\text{B}} C \langle n_{\text{H}} \rangle^2 R^3}{4\pi c x_{\text{HI}} \langle n_{\text{H}} \rangle R^2 + \dot{N}_{\text{phs}} - \frac{4\pi}{3} \alpha_{\text{B}} C \langle n_{\text{H}} \rangle^2 R^3} \quad (10)$$

where  $\dot{N}_{\text{phs}} = \dot{N}_{\text{phs}}(\tau) = \dot{N}_{\text{phs}}(t_A - t_i - R/c)$ . At  $\theta = 0$

we have  $\tau = \tau_Q$  (eq. 3) and thus  $\dot{N}_{\text{phs}}$  is simply  $\dot{N}_{\text{phs}}(\tau_Q)$ ; at  $\theta = \pi/2$  we have  $\tau = \tau_Q - R/c$  and thus  $\dot{N}_{\text{phs}}$  is simply  $\dot{N}_{\text{phs}}(\tau_Q - R/c)$ . Note that in principle the apparent ionization front at  $\theta = \pi/2$  may not necessarily correspond to the maximum angle of the apparent ionized region extended on the sky (see Fig. 1).

Note that in equation (7)  $\dot{N}_{\text{phs}}(\tau)$  is a non-decreasing function of  $\tau$  so that  $r(\tau)$  expands with increasing  $\tau$ . When  $\dot{N}_{\text{phs}}(\tau)$  decreases with increasing  $\tau$  (e.g., close to the quenching of the QSO nuclear activity) and  $\tau \gg \tau_{\text{rec}}$ , the ionization front shrinks, and its evolution may not be described by equation (7) if the characteristic decreasing timescale of  $\dot{N}_{\text{phs}}(\tau)$  is significantly short compared to the recombination timescale. For simplicity, in this paper we ignore the decreasing phase of the QSO luminosity evolution, which has been shown to at least not dominate the main population of luminous QSOs observed at relatively low redshifts (Yu & Lu 2004).

Below we assume two simple models of  $\dot{N}_{\text{phs}}(\tau)$  (see also Yu & Lu 2005): in model (i)  $\dot{N}_{\text{phs}}(\tau) = \dot{N}_{\text{phs},i}$  is a constant, and in model (ii)  $\dot{N}_{\text{phs}}(\tau) = \dot{N}_{\text{phs},i} \exp(\tau/\tau_S)$  increases exponentially with  $\tau$ , where  $\tau_S \simeq 4.5 \times 10^7 \text{ yr} [0.1\epsilon/(1-\epsilon)]$  is the Salpeter timescale and  $\epsilon$  is the mass-to-energy conversion efficiency. When  $\tau \ll \tau_{\text{rec}}$  in model (i) or  $\tau \ll \min\{\tau_{\text{rec}}, \tau_S\}$  in model (ii), the effects of recombination and the evolution of the QSO luminosity are both negligible and  $r(\tau)$  is given by

$$r(\tau) \simeq \left( \frac{3\dot{N}_{\text{phs},i}\tau}{4\pi x_{\text{HI}} \langle n_{\text{H}} \rangle} \right)^{1/3} = r_S \left( \frac{\tau}{\tau_{\text{rec}}} \right)^{1/3}, \quad (11)$$

where

$$r_S \equiv \left( \frac{3\dot{N}_{\text{phs},i}\tau_{\text{rec}}}{4\pi x_{\text{HI}} \langle n_{\text{H}} \rangle} \right)^{1/3} = \left( \frac{3\dot{N}_{\text{phs},i}}{4\pi \alpha_{\text{B}} C \langle n_{\text{H}} \rangle^2} \right)^{1/3}. \quad (12)$$

Given equation (11), the changing rate of  $r(\tau)$  with  $\tau$  is larger than  $c$  if  $\tau \lesssim [r_S/(3c\tau_{\text{rec}})]^{3/2} \tau_{\text{rec}}$  (i.e.,  $r(\tau) \gtrsim 3c\tau$  here). As the ionization front expands, if  $\tau \gg \tau_{\text{rec}}$  (and  $\tau_{\text{rec}} \ll \tau_S$  in model ii), the recombination within the highly ionized H II region is approximately balanced by the emission of the ionizing photons from the QSO, and we have

$$r(\tau) \simeq \begin{cases} r_S & \text{for model (i),} \\ r_S \left( \frac{\tau_S}{\tau_{\text{rec}} + \tau_S} e^{\tau/\tau_S} \right)^{1/3} & \text{for model (ii),} \end{cases} \quad (13)$$

which is insensitive to the detailed value of  $\tau$  for model (i) and depends on  $\tau$  only through  $N_{\text{phs}}(\tau)$  in model (ii). In case that  $\tau_{\text{rec}} \gg \tau_S$  in model (ii),  $r(\tau)$  at  $\tau \gg \tau_S$  still follows equation (13), but the effect of recombination is not important and  $r(\tau)$  is mainly determined by the QSO emission. Given equation (13), for the exponential increase of the luminosity evolution in model (ii), the changing rate of  $r(\tau)$  with  $\tau$  is larger than  $c$  if  $r(\tau) \gtrsim 3c\tau_S$ .

#### 4. THE EVOLUTION OF THE APPARENT SHAPE OF THE IONIZATION FRONT

By combining equations (3) and (8), we obtain the evolution of the apparent shape of the ionization front  $(r, \theta)$  for different models of the QSO luminosity evolution, which is shown in Figure 2. The evolution of the

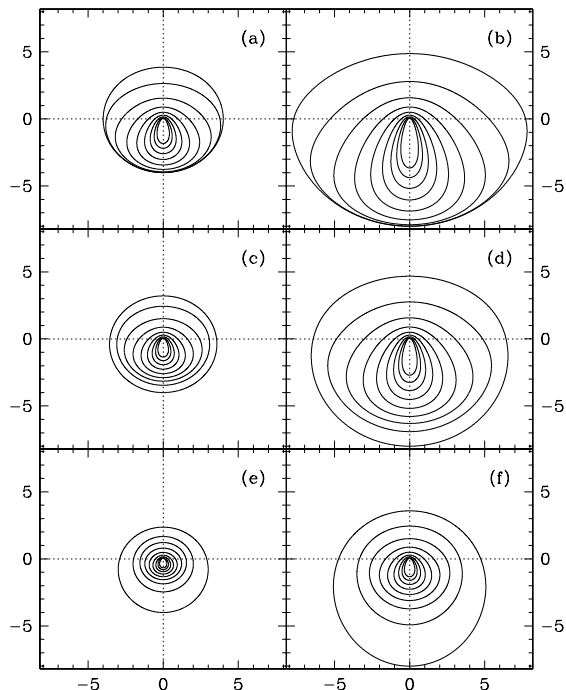


FIG. 2.— Expected evolution of the apparent shape of the ionization front around a QSO. The geometric configuration of the QSO (located at the crossing point of the dotted lines) and the observer is the same as in Figure 1. The QSO emission is assumed to be isotropic. Both of the axes are in units of  $c\tau_{\text{rec}}$  (see  $\tau_{\text{rec}}$  in eq. 9). Top panels (a)-(b) are for model (i) of  $\dot{N}_{\text{phs}}$  (see § 4), and middle and bottom panels for model (ii) with  $\tau_S/\tau_{\text{rec}} = 10$  (c-d) and 3 (e-f), respectively. The parameters  $(\dot{N}_{\text{phs},i}, \langle n_{\text{H}} \rangle, C)$  are set so that  $r(\tau = 10\tau_{\text{rec}})/(c\tau_{\text{rec}}) = 4$  in the left panels (a,c,e) and 8 in the right panels (b,d,f). In each panel, different curves represent the apparent shapes with different  $\tau_Q/\tau_{\text{rec}}$ . The  $\tau_Q/\tau_{\text{rec}}$  increases from inward to outward with  $\delta \log(\tau_Q/\tau_{\text{rec}}) = 0.25$ , and the outmost curve has  $\tau_Q/\tau_{\text{rec}} = 10$ .

apparent shape and size depends on the QSO luminosity evolution and its environment (e.g., the hydrogen reionization history or structure formation) through the parameters  $(\tau_Q, \tau_S, \tau_{\text{rec}}, r_S)$ . In Figure 2, the parameters  $(\dot{N}_{\text{phs},i}, x_{\text{HI}}, C, \langle n_{\text{H}} \rangle)$  are set so that  $r_S/(c\tau_{\text{rec}})$  is larger in the right panels than in the left ones. Top panels (a) and (b) are for model (i) of  $\dot{N}_{\text{phs}}(\tau)$ . As seen from them, the apparent shapes of the ionization fronts are generally not a sphere, especially if  $\tau_Q$  is short (inner curves) and  $r_S/(c\tau_{\text{rec}})$  is large (e.g., because  $\dot{N}_{\text{phs},i}$  is high or  $x_{\text{HI}}$  is low; right panel). The apparent shape expands as  $\tau_Q$  increases. When  $\tau_Q$  is long enough, the apparent shape at small  $\theta$  (see the definition of  $\theta$  in Fig. 1) starts to be almost independent of  $\tau_Q$  and approaches a sphere, since the radius of the Strömberg sphere approaches the equilibrium value  $r_S$  (eq. 13) at which the ionizing photon emission is balanced by the recombination. With increasing  $\tau_Q$ , the shape at large  $\theta$  continues to expand and finally the whole apparent shape becomes spherical (see the outmost curve in panel a). According to equation (12), the stronger the  $\dot{N}_{\text{phs},i}$  or the smaller the  $C$ , the larger the final equilibrium sphere radius. In addition, in case that  $r_S/(c\tau_{\text{rec}})$  is significantly small ( $\ll 1$ ), the expansion may become non-relativistic at a time much earlier than  $\tau_Q \simeq \tau_{\text{rec}}$ , thus the apparent shape may ap-

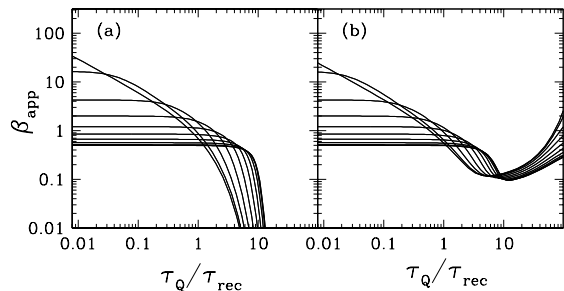


FIG. 3.— Expected apparent radial expansion speed of the ionization front in units of  $c$  as a function of  $\tau_Q/\tau_{\text{rec}}$  (eq. 4). Panel (a) (model i of  $\dot{N}_{\text{phs}}$ ) has the same parameters as those in Figure 1a, and panel (b) (model ii) the same as those in Figure 1c. In each panel, different curves give the speeds at different  $\theta$ , which increases from 0 to  $180^\circ$  with  $\delta\theta = 30^\circ$  from top to bottom at the low- $\tau_Q/\tau_{\text{rec}}$  end. The apparent speed at small  $\theta$  is superluminal at small  $\tau_Q/\tau_{\text{rec}}$  in both panels and also at large  $\tau_Q/\tau_{\text{rec}}$  for model (ii) in panel (b). For simplicity, we do not show the apparent transverse expansion speed  $\beta_{\text{app},\perp} = \beta_{\text{app}} \sin \theta$  here, which also gives the similar superluminal phenomenon except at  $\theta = 0$ .

proach a sphere even if  $\tau_Q \ll \tau_{\text{rec}}$  (but  $\tau_Q > r(\tau_Q)/(3c)$ ). Figure 2c-f illustrate the apparent shapes for model (ii) of  $\dot{N}_{\text{phs}}(\tau)$ , where the timescales of increasing luminosity are set to have  $\tau_S/\tau_{\text{rec}} = 10$  and 3, respectively. In model (ii) the size of the apparent shape is sensitive to  $\tau_Q$  even if  $\tau_Q$  is long because  $\dot{N}_{\text{phs}}$  increases with time exponentially; and the shape does not evolve towards a spherical shape, especially if  $\tau_S$  is small (bottom panels e-f).

For the realistic case of the highest redshift QSOs with Gunn-Peterson troughs observed so far ( $z \sim 6.1 - 6.4$ ; Fan 2004; White et al. 2003), Yu & Lu (2005) study the environmental effect of their surrounding regions and obtain  $x_{\text{HI}} \sim 0.1$  and  $C \sim 30 - 40$  (which are shown to be consistent with the observed Strömberg radii). Then the recombination timescale  $\tau_{\text{rec}}$  is  $\sim 4 \times 10^6$  yr (eq. 9), which is significantly shorter than the QSO lifetime ( $\gtrsim 4 \times 10^7$  yr; e.g., Yu & Lu 2004). Thus the ages of most observed QSOs should be long enough that the sizes of the ionization fronts along the line of sight are close to the equilibrium values. For the observed QSOs with  $\dot{N}_{\text{phs}}(\tau_Q) \sim 10^{57} \text{ s}^{-1}$ , the apparent size at  $\theta = 0$  is  $r(\tau_Q) \sim 5 \text{ Mpc}$  ( $\sim 3 - 4c\tau_{\text{rec}}$ ) (Yu & Lu 2005), and the apparent shapes should be close to the outer curves shown in Figure 2a and c (see also Fig. 4 if the QSO emission is anisotropic). Statistically a small fraction of observed QSOs would also have significantly short ages and the apparent shapes of their ionization fronts should systematically deviate from a spherical shape (see the inner curves in Fig. 2). Wyithe & Loeb (2004a) obtain a much higher  $x_{\text{HI}}$  and a low QSO age from the observed Strömberg radius of a QSO by using a much smaller clumping factor; in this case, the recombination timescale is significantly long (up to  $10^9$  yr) and  $r(\tau_Q)$  is not significantly smaller than  $3c\tau_Q$ , so the apparent shapes of most observed QSOs should be more likely to systematically deviate from a spherical shape.

Using equation (5), we illustrate the apparent expansion speed of the ionization front as a function of  $\tau_Q$  in Figure 3. Panel (a) is for model (i) of  $\dot{N}_{\text{phs}}$  and panel (b) for model (ii). As seen from Figure 3, the speed is su-

perluminal at small  $\theta$  and  $\tau_Q/\tau_{\text{rec}}$ . For the specific case of  $\theta = 0$ , we have  $\tau = \tau_Q$  and  $\beta_{\text{app}} = c^{-1}dr/d\tau$  (eqs. 3 and 4), and the corresponding superluminal expansion is also mentioned or discussed in some recent literature (Cen & Haiman 2000; White et al. 2003; Wyithe & Loeb 2004b). In panel (b), the speed at small  $\theta$  may also become superluminal even at large  $\tau_Q/\tau_{\text{rec}}$  because the ionizing photon emission rate and  $r(\tau)$  (eq. 13) increases exponentially in model (ii). The expansion of the highly ionized regions around the highest redshift QSOs with Gunn-Peterson troughs provides another astrophysical example of the superluminal phenomenon (for other examples, e.g., see reviews in Blandford, McKee & Rees 1977; Falla, Floyd, & Potter 2003).

### 5. EFFECTS OF ANISOTROPY OF QSO EMISSION

In the above, QSO ionizing photons have been assumed to be emitted isotropically. However, in reality the QSO emission may be anisotropic at least in these two cases: (i) a torus is surrounding the central black hole in the QSO, which blocks the ionizing photons from the central engine; (ii) the UV ionizing photon emission from the accretion disk surrounding the black hole is anisotropic (see also discussions of the effects of anisotropy of QSO emission in Cen 2003 and Wyithe & Loeb 2004b).

In case (i), the highly ionized region in the rest frame of the QSO may appear simply like a large-scale version of the [OIII] ionization “cone” detected in local Seyfert 2 galaxies. The expected apparent shape is easily correspondingly adjusted depending on the normal direction and the opening angle of the torus.

In case (ii), we assume that the emergent intensity from the accretion disk is  $\propto (1 + 2|\mu|)$  because of the limb-darkening effect (e.g., Krolik 1999), where  $\mu$  is the cosine of the angle between the disk normal and the emitting direction (so far there is no much evidence to show that UV photons from QSOs are strongly beamed). Here the QSO anisotropic emission is symmetric about the disk plane and axisymmetric about the disk normal. Although both the relativistic time-delay and the anisotropy of the QSO emission may make the apparent shape deviate from a spherical shape, their effects are different. As mentioned above, the time-delay effect decreases  $r(\tau)$  with increasing  $\theta$  (see eq. 3) and does not break the rotational symmetry of the ionized region about the observer’s line of sight  $\vec{OC}$ . For the anisotropic effect here, the detailed dependence of the apparent size on  $\theta$  is significantly affected by the detailed geometric configuration between the accretion disk and the observer. The rotational symmetry of the apparent shape around the observer’s line of sight is generally broken unless the disk normal is coincident with the observer’s line of sight. We denote the angle between the disk normal and the observer’s line of sight by  $\theta'$  ( $0 \leq \theta' \leq \pi/2$ ). For  $\theta' \neq 0$ , the cross sections of the apparent ionized region are illustrated in Figure 4, where the observer’s line of sight is on the cross section,  $\phi$  ( $0 \leq \phi < \pi$ ) is the angle of the cross section anti-clockwise from the plane in which  $\vec{OC}$  and the disk normal are located, and  $|\mu| = |\sin \theta \cos \phi \sin \theta' \pm \cos \theta \cos \theta'|$ . Although in general  $r(\tau)$  does not necessarily decrease with increasing  $\theta$  if the QSO emission is anisotropic, the apparent size in any direction from the central QSO with  $\theta < \pi/2$  is still systematically not larger than the size in

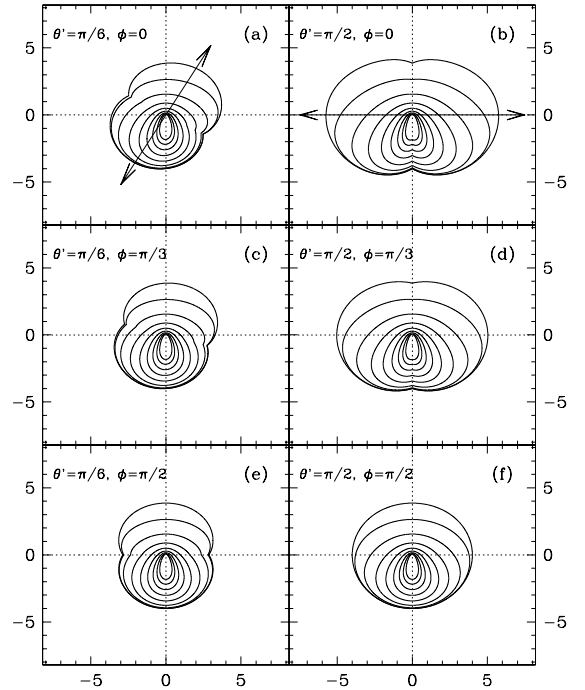


FIG. 4.— Cross sections of the apparent ionized region after including the anisotropy of the accretion disk emission due to the limb-darkening effect in Figure 2a. The solid lines with arrows in (a) and (b) are the disk normal passing the QSO. The emission is assumed to be symmetric about the disk plane and rotationally symmetric about the disk normal. The parameters ( $\dot{N}_{\text{phs},i}, \langle n_{\text{H}} \rangle, C$ ) are set so that  $r[\tau(10\tau_{\text{rec}}, \theta = 0)] = 4$ . After including the anisotropic effect, the rotational symmetry about the observer’s line of sight mentioned in Figure 1 is broken, so the cross sections are different in the top, middle, and bottom panels. As in Figure 1, for each curve, the apparent size in any direction from the central QSO with  $\theta < \pi/2$  is not smaller than the size in the opposite direction due to the time-delay effect. See details in § 5.

the opposite direction because of the time-delay effect and the symmetry assumed for the anisotropic emission here. Given the detailed discussions in § 4, if the QSO age is significantly long compared to the hydrogen recombination process and the QSO luminosity evolution is significantly slow, the apparent ionized region follows the same symmetry as the QSO emission (i.e., symmetric about the disk plane and axisymmetric about the disk normal here). As seen from Figure 4, the smaller the  $\tau_Q/\tau_{\text{rec}}$  and the smaller the  $\theta'$ , the less important the anisotropic effect.

### 6. POSSIBLE OBSERVATIONAL TESTS

We use Figure 1 to illustrate the possible observational tests of the apparent shape. The discussion below may be generalized to the anisotropic case of QSO emission.

If there exists a background object  $S$  behind the highly ionized region (see Fig. 1), significant transmission of Ly $\alpha$  (and/or Ly $\beta$ ) photons may be present on the Gunn-Peterson trough in the observational spectrum of  $S$  at wavelengths corresponding to redshifts  $z(t_A)$  to  $z(t_B)$  [somewhat like (but it may be much broader than) the observed emission spike on top of the Gunn-Peterson trough of SDSS J1148+5251; see Figs. 4 or 5 in White et al. 2003]. Similarly, the spectra of background objects lying inside the highly ionized regions (see also discussions for inside objects in Cen 2003) may also show

transmission features of Ly $\alpha$  photons at the wavelength corresponding to the redshift when its light travels out of the ionized region. If the background object is the QSO itself, we have  $\tau = \tau_Q$  at  $\theta = 0$  (eq. 3) and the size of the apparent ionization front  $|OC| = r(\tau_Q)$ , which can be measured directly from the wavelength difference between the Gunn-Peterson trough and the Ly $\alpha$  line center in the QSO spectrum (e.g., White et al. 2003). Note that the existence of Ly $\alpha$  emitting galaxies lying behind or inside the highly ionized regions of the highest redshift QSOs is likely and detection of them is possible by current techniques, since the apparent “Strömgren sphere” with a physical size  $\sim 5$  Mpc at  $z \sim 6$  covers an area about  $14 \times 14$  arcmin<sup>2</sup> on the sky and is large enough for this compared to the survey areas of some Ly $\alpha$  surveys (see Table 1 in Stern et al. 2004) that have successfully discovered galaxies at  $z \sim 6.5$ . By obtaining observational spectra of a number of background sources with different projecting distances ( $R_\perp = |OA| \sin \theta$ ) to the highest redshift QSO(s), one can measure the proper distance of  $|AB|$  (or  $|OA|$ ,  $|OB|$ ) for each source behind the region(s) (or  $|OB|$  for inside sources) and then statistically map the three-dimensional apparent shape of the highly ionized region(s) surrounding the QSO(s). The distribution of these distances as a function of  $R_\perp$  may be used to statistically constrain the evolution of the apparent ionization fronts (and hence the QSO luminosity evolution and its environment), as illustrated in Figure 5.

In addition, the apparent shape of the highly ionized region surrounding the QSOs with Gunn-Peterson troughs might also be revealed by radio surveys of the hyperfine transition 21 cm line emission of neutral hydrogen (e.g., the Low Frequency Array, the Square Kilometer Array, the Primeval Structure Telescope, the Mileura Wide-Field Array), a possible technique to map the neutral hydrogen distribution at high redshift (see discussions in Wyithe & Loeb 2004b).

For the observer on Earth, the physical distance of  $R_\perp$  can be obtained by  $R_\perp = D_A \delta\phi$ , where  $D_A$  is the angular diameter distance to the QSO and  $\delta\phi$  is the angle of the QSO and the ionization front (e.g., point  $A$ ) separated on the sky. The transformation of the angular and the redshift space to real space ( $R_\perp$  and  $|AB|$ ,  $|OA|$  or  $|OB|$  etc.) depends on the cosmological parameters. If the QSO age and environment are effectively constrained by the apparent ionization front (through  $|OC|$ ,  $|AB|/|OC|$  etc.) at small  $R_\perp \sim 0$  and if the anisotropy of QSO emission is effectively constrained by some cross sections of the apparent ionized region, the apparent physical sizes of the ionized region at other directions may be predicted by using the method in this paper. Thus, the ratio of the redshift difference between the QSO and the apparent ionization front at  $R_\perp \sim 0$  to the maximum angle(s) of the apparent ionized region (or cross sections) extended on the sky might be used to provide constraints on the cosmological parameter  $\Omega_\Lambda$  by the Alcock-Paczyński test (Alcock & Paczyński 1979), since the angular size significantly depends on  $\Omega_\Lambda$  but the redshift size does not at  $z \sim 6$ .

## 7. CONCLUSIONS

In this paper we have illustrated the apparent shape of the ionization front around the highest redshift QSOs, and its evolution, with Gunn-Peterson troughs in the

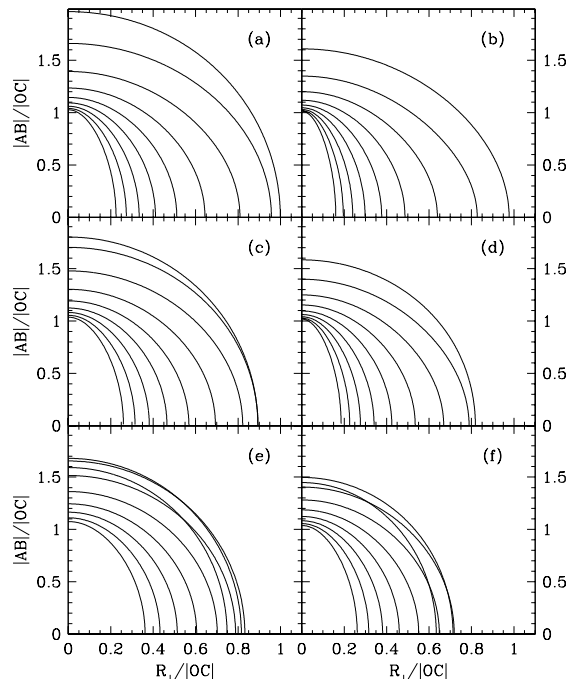


FIG. 5.— Expected ratio of  $|AB|/|OC|$  of the apparent ionization front as a function of  $R_\perp/|OC|$  (see Fig. 1 for the definition of the proper distances of  $|AB|$ ,  $|OC|$ , and  $R_\perp$ ). The parameters are the same as those in Figure 2. This figure illustrates that the evolution of the apparent ionization fronts around QSOs may be inferred from the distribution of  $|AB|$ . For observational methods of determining  $|AB|$  and  $|OC|$ , see discussion in § 6. A similar study may also be done for  $|OA|$  and  $|OB|$ .

spectra. We have shown that the apparent shape and its evolution depend on the age and the luminosity evolution of the QSO, the recombination process of ionized hydrogen surrounding the QSO, and the anisotropic property of the QSO emission. Both the relativistic time-delay effect and the anisotropy of QSO emission may make the apparent shape deviate from a sphere. The time-delay effect systematically makes the apparent size of the ionization front in the directions away from the observer smaller than the size in the directions towards the observer. The deviation of the shape caused by the time-delay effect is not significant if the QSO age is significantly long compared to the hydrogen recombination process within the ionization front and the QSO luminosity evolution is significantly slow. The time-delay effect does not break the rotational symmetry of the ionized region about the observer’s line of sight to the QSO. The apparent expansion of the ionization front may be superluminal at the early stage of its expansion or if the QSO ionizing photon emission rate increases dramatically (e.g., exponentially). The anisotropic effect on the apparent shape depends on the detailed anisotropy of the emission (e.g., affected by the normal direction of the accretion disk in the QSO) and may break the rotational symmetry about the observer’s line of sight.

The apparent shape of the highly ionized regions may be mapped by transmitted spectra of background sources behind or inside them or by surveys of the hyper-fine transition 21 cm line of neutral hydrogen. The apparent shape could also be used to constrain the cosmological parameter  $\Omega_\Lambda$  by the Alcock-Paczyński test.

I am grateful to Youjun Lu for helpful discussions and thoughtful comments. I thank Ue-Li Pen for helpful discussions. QY acknowledges support provided by NASA through Hubble Fellowship grant #HF-01169.01-

A awarded by the Space Telescope Science Institute, which is operated by the Association of Universities for Research in Astronomy, Inc., for NASA, under contract NAS 5-26555.

#### REFERENCES

- Adelberger, K. L. 2004, *ApJ*, 612, 706  
 Alcock, C., & Paczyński, B. 1979, *Nature*, 281, 358  
 Bajtlik, S., Duncan, R. C., & Ostriker, J. P. 1988, *ApJ*, 327, 570  
 Blandford, R. D., McKee, C. F., & Rees, M. J. 1977, *Nature*, 267, 211  
 Cen, R. 2003, *ApJ*, 597, 13  
 Cen, R., & Haiman, Z. 2000, *ApJ*, 542, L75  
 Couderc, P. 1939, *Ann. Astrophys.*, 2, 271  
 Donahue, M., & Shull, J. M. 1987, *ApJ*, 323, L13  
 Falla, D. F., Floyd, M. J., & Potter, A. G. 2003, *European Journal of Physics*, 24, 197  
 Fan, X. et al. 2002, *AJ*, 123, 1247  
 Fan, X. et al. 2004, *AJ*, 128, 515  
 Krolik, J. H. 1999, *Active Galactic Nuclei: From the Central Black Hole to the Galactic Environment* (Princeton: Princeton Univ. Press)  
 Madau, P., & Rees, M. J. 2000, *ApJ*, 542, L69  
 Mesinger, A., & Haiman, Z. 2004, *ApJ*, 611, L69  
 Pentericci, L., et al. 2002, *AJ*, 123, 2151  
 Rees, M. J. 1966, *Nature*, 211, 468  
 Rees, M. J. 1967, *MNRAS*, 135, 345  
 Shapiro, P. R., & Giroux, M. L. 1987, *ApJ*, 321, L107  
 Stern, D., Yost, S. A., Eckart, M. E., Harrison, F. A., Helfand, D. J., Djorgovsky, S. G., Malhotra, S., & Rhoads, J. E. 2004, *ApJ*, in press, astro-ph/0407409  
 White, R. L., Becker, R. H., Fan, X., & Strauss, M. A. 2003, *AJ*, 126, 1  
 Wyithe, J. S. B., & Loeb, A. 2004a, *Nature*, 427, 815  
 Wyithe, J. S. B., & Loeb, A. 2004b, *ApJ*, 610, 117  
 Yu, Q., & Lu, Y. 2004, *ApJ*, 602, 603  
 Yu, Q., & Lu, Y. 2005, *ApJ*, 620, 31